Journal of Engineering Science and Technology Review 18 (2) (2025) 132- 139

Research Article

JOURNAL OF
Engineering Science and Technology Review

www.jestr.org

A Comparison of Polar Coded 5G NR waveforms-UFMC, F-OFDM, and FBMC in Massive MIMO system

Smita Jolania[1,*], Ravi Sindal[1] and Ankit Saxena[2]

[1]*Institute of Engineering and Technology DAVV, Indore, India*
[2]*Indore Institute of Science and Technology, Indore, India*

Received 11 October 2024; Accepted 28 February 2025

Abstract

Fifth-generation (5G) mobile networks have the potential to provide seamless connectivity for massive devices with a significantly improved quality of service. In this context, new modulation and coding schemes in small-cell deployment scenarios are implemented at the physical layer of 5G New Radio (NR). With their proven flexibility, Polar codes have emerged as the most adaptable coding technique, achieving Shannon capacity and reducing complexity, targeting mainly control channels. This adaptability of 5 G technology reassures us that it can seamlessly adapt to various scenarios, providing a versatile solution for diverse communication needs. Additionally, more freedom for coordination, Multiple Antenna Technology, and Massive Multiple Input and Multiple Output (MIMO) provide the vertical spatial domain, where 100 antennas are installed at next-generation Node B (gNB). In this paper, the complete framework for 5G New Radion (NR) based waveforms Filtered-Orthogonal Frequency Division Multiplexing (F-OFDM), Filter Bank Multicarrier (FBMC), and Universal Filtered Multi-Carrier (UFMC) systems are designed with Polar coding. Simulation results proved that the Bit Error Rate (BER) performance of the proposed polar-coded UFMC system is better than polar-coded FBMC and polar-coded F-OFDM by achieving SNR gain of approximately ~2dB and ~12 dB, respectively, over these waveforms in 32x16 MIMO setup.

Keywords: Massive MIMO, FBMC, UFMC, F-OFDM, Polar codes

1. Introduction

The major services of 5G networks are enhanced mobile broadband (eMBB), massive Machine Type Communication (mMTC), and ultra-reliable Low latency Communication (uRLLC) [1,2]. The 5G network must perform in a limited spectrum with high data rate, variable traffic, and high reliability. The key candidates contributing to the enhancement of the capacity of next-generation wireless communications systems are Air interface comprising new modulation and coding scheme, 3D-MIMO, more Licensed and Unlicensed Spectrum, Millimeter-Wave Bands, Cell Densification, Device-to-Device communication, etc. [3]. The air interface defined in 5G-NR is a major transition to support dynamic and flexible service requirements. In the standards defined for 5G-NR, Waveforms are designed by Orthogonal Frequency Division Multiplexing (OFDM) with potential support of the non-orthogonal waveform proposed. To further enhance reliability, flexible channel coding techniques facilitate variable information block and codeword size with rate matching [4].

The multi-carrier waveforms in 5G must be designed to have low spectral leakage and peak-to-average-power ratio (PAPR) [5]. OFDM, the critical candidate of the Fourth Generation (4G) system, has numerous flaws. Mainly, it suffers from high PAPR, carrier frequency offset (CFO), etc. [6]. 5G-NR proposes various new multicarrier waveforms that provide flexibility and scalability to serve heterogeneous application areas. Major 5G waveform candidates are FBMC [7], Generalized Frequency Division Multiplexing (GFDM) [8], UFMC [9], and F-OFDM [10].

Channel coding techniques in 5G NR should support block size, code rate, and codeword size flexibility. In 5G, the Channel coding must be redefined entirely to meet its diversified requirements [11]. Polar codes proposed in 2009 by Arikan [12] proved to be capacity-achieving codes in any Binary Memoryless Symmetric (BMS) channel with less complex encoded and decoding algorithms. 5G NR air interface and Massive MIMO technology can effectively increase the capacity and fulfil the enormous traffic demands of 5G networks [13]. In Massive MIMO, 100s of antennas are implemented at the base station (referred to as gNodeB (gNB) in 5G NR terminology) to improve the network capacity and throughput [14]. T.L. Marzetta introduced the concept of massive MIMO in [15] and concluded that asymptotically, as the number of antennas at gNB$\rightarrow \infty$, the system processing gain tends to infinity. The hybrid system of Massive MIMO with Polar coding and various 5G NR waveforms is designed and compared.

2. Motivation and Scope

Designing systems with advanced waveforms like F-OFDM, FBMC, and UFMC is motivated by their ability to enhance spectrum efficiency and meet diverse service demands. Polar coding, recognised for its ability to approach Shannon capacity, ensures efficient error correction and reliability, particularly in control channel operations. Incorporating technologies such as Multiple Antenna Technology and Massive MIMO opens avenues for spatial diversity and improved performance in scenarios involving a large number of antennas (e.g., at gNB).

*E-mail address: sprajapati2911@gmail.com
ISSN: 1791-2377
doi:10.25103/jestr.182.17

The objective is to develop and evaluate F-OFDM, FBMC, and UFMC waveforms tailored to meet the unique demands of 5G NR applications. This work will focus on interference reduction, spectral efficiency, and latency improvements. The simulation results have investigated the interplay between advanced waveform designs and cutting-edge technology like massive MIMO.

The rest of the document is framed as follows: In section II, 5G NR waveforms are presented with mathematical models of filters. This includes FBMC, UFMC, and F-OFDM modulation waveforms. Section III gives an overview of polar encoding and decoding. Then, section IV elaborates on the proposed polar-coded waveforms with a massive MIMO scenario over the Rayleigh channel. Section V covers the system design aspects with simulation parameters and the results. Lastly, the performance analysis is concluded in section VI. The paper's significant contribution is that the BER and PSD performance of Polar coded waveforms with massive MIMO antenna arrays is evaluated and compared.

3. Major Design Methods

3.1 FBMC-Offset-QAM

FBMC is based on subcarrier filtering in the frequency domain. In FBMC, the bandwidth is divided into subcarriers, and filtering is applied on a subcarrier basis, making it more flexible with improved out-of-band (OOB), thereby enhancing the spectral efficiency [16]. The study in [17] has proved that the FBMC technique is resilient in controlling bandwidth using subcarrier-wise filtering [18]. The FBMC can use Quadrature Amplitude Modulation (QAM) signaling or offset QAM (OQAM) signaling. In OQAM, the QAM symbols are bifurcated into real and imaginary parts. To avoid simultaneous transmission of real and imaginary symbols, imaginary symbols are delayed half the duration of the symbol concerning the real symbols. As a result, the OQAM symbol rate is twice the QAM symbol rate. FBMC-OQAM proved to have optimal spectral localization, reducing the inherent overheads by the extended filter without cyclic prefix (CP) or guard period [19-20].

Fig. 1 illustrates the FBMC transmitter block. The FBMC-OQAM transmitter comprises the Synthesis Filter Bank (SFB) [21].

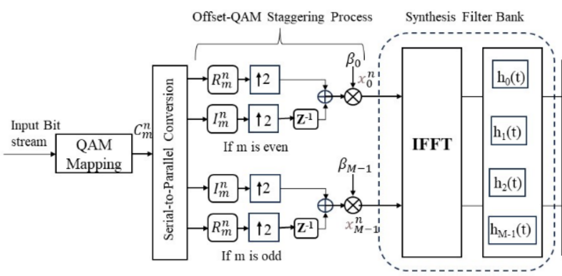

Fig. 1. FBMC-OQAM Modulator Design

Initially, the random data is generated and mapped into the QAM symbol. The complex input symbol is shown in equation (1):

$$C_m^n = R_m^n + iI_m^n \tag{1}$$

Here $0 < n \leq N-1$. Given that N is the number of subcarriers and $0 < m \leq M-1$, M complex input symbol. R_m^n and I_m^n are the real and imaginary parts of the mth symbol on the nth subcarriers, respectively. The mth symbols on all subcarriers form a data block as follows in equation (2):

$$C_m = [C_m^0, C_m^1, \dots . C_m^{N-1}]^T \tag{2}$$

The OQAM and Nyquist conditions are used on the prototype filter to ensure orthogonality with enhanced spectral efficiency. The complex-valued QAM symbols' in-phase and quadrature components are staggered during the pre-processing [22]. The significant point is that the quadrature component is delayed on even subcarriers, while the real part is delayed on odd subcarriers. The time domain version of the modulated signal can be expressed as equation (3):

$$s\,(t) = \sum_{m=0}^{2M-1}\sum_{n=0}^{N-1} x_m^n h(t - \frac{mT}{2}) e^{j(\frac{2\pi}{T}nt+\varphi_m^n)} \tag{3}$$

where x_m^n is the mapping signal whose property is shown by equation (4), and h(t) is the impulse response of the prototype filter.

$$x_m^n = \begin{cases}(1-\delta)R_m^n + \delta I_m^n, & if\ m\ is\ even\\ \delta R_m^n + (1-\delta)I_m^n, & if\ m\ is\ odd\end{cases} \tag{4}$$

Here $\delta\epsilon$ {1,0}, and $\beta_m = e^{j\varphi_m^n}$ is a phase term to be $\varphi_m^n = \frac{\pi}{2}(m+n) - \pi mn$. OQAM mapping lowers ICI when suitable filters are used. In FBMC, the prototype filter is designed with overlapping factor K where the filter length L = K $*$ N, N=size of FFT. As a result, each FBMC symbol in the time domain overlaps with K neighboring symbols. Due to overlapping, the filter's impulse response must be governed by the Nyquist criterion to avoid inter-symbol interference [23]. CP in FBMC is replaced with filter banks. This paper considers the PHYDYAS [21] filter based on frequency sampling technology as the prototype filter.

The M subcarriers frequency response of the PHYDYAS filter is given by equation (5):

$$H\,(f) = \sum_{k=-(K-1)}^{K-1} H_k \frac{\sin\,(\pi\left(f-\frac{k}{MK}\right)MK)}{MK\,\sin\,(\pi\left(f-\frac{k}{MK}\right)MK)} \tag{5}$$

Where Hk is the coefficient impulse response, k is the subcarrier index—the frequency domain coefficient of the filter as shown in Table 1.

Table 1. Frequency domain prototype filter coefficients [21]

K	H0	H1	H2	H3
2	1	0.707106	-	-
3	1	0.911438	0.411438	-
4	1	0.971960	0.707106	0.235147

The impulse response of the filter after the Inverse Fast Fourier Transform (IFFT) processing is given by equation (6):

$$h(t) = 1 + 2\sum_{k=1}^{K-1} H_k \cos\left(2\pi\frac{kt}{KT}\right) \tag{6}$$

The Analysis Filter Bank (AFB), constructed by M analysis filters, is used at the receiver side. After filtering, the signal is down-sampled by a factor of 2 to form an output signal. Prototype filter banks filter the original signal with different offsets [22]. The receiver design is shown in Figure 2.

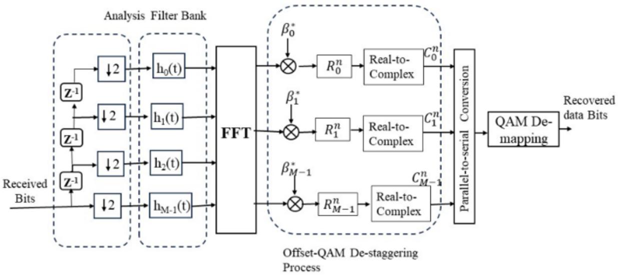

Fig. 2. FBMC/OQAM Receiver Design

3.2. Universal Filtered Multi-Carrier (UFMC)

In Universal filtered multicarrier (UFMC), sub-band filtering is applied. Here, the available carriers are divided into N sub-bands. This waveform uses filters at the transmitter and receiver to shape the subcarrier waveforms and achieve a more flexible frequency localization. The significant aspects of UFMC include Filtered Subcarriers, Subcarrier Overlapping, Low Interference, and Flexible Resource Allocation. UFMC offers better ICI robustness and flexibility for sub-band fragmentation [24]. The shorter filter lengths compared to FBMC make it applicable for short-block communication. The UFMC transmitter block is shown in Figure. 3.

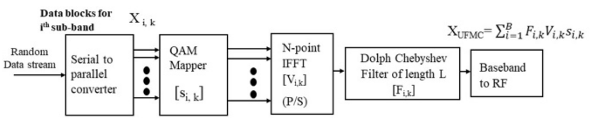

Fig. 3. UFMC Transmitter Design

The available subcarriers are divided into sub-bands, each of K subsequent subcarriers. These subcarriers are QAM-modulated, generating complex symbols. The modulated symbols in each sub-band are then converted into the time domain using an N-IFFT module [25]. Each sub-band is filtered using a Dolph-Chebyshev filter, reducing the spectral leakage and ICI.

The Chebyshev window is expressed by equation (7):

$$F_{i,k}=\frac{\cos\{N.cos^{-1}[\beta\cos(\frac{\pi k}{N})]\}}{\cos[N\,cosh^{-1}(\beta)]} \tag{7}$$

Where k ranges from 0 to (N-1), $\beta = \cosh\{\frac{1}{N}\cosh^{-1}(10^{\alpha})\}$. The 'α' is the side lobe attenuation factor in dB=−20α [where α= (2,3,4)] [26]. The UFMC signal can be represented as shown in equation (8):

$$X_K = \sum_{i=1}^{B} F_{i,k}V_{i,k}s_{i,k} \tag{8}$$

B is the number of sub-bands, $S_{i,k}$ is a vector of QAM symbols, $V_{i,k}$ is the IFFT matrix, and $F_{i,k}$ is the Toeplitz matrix of the filter. The signal will follow the time domain pre-processing to suppress interference at the receiver end. Figure 4 shows the UFMC receiver section.

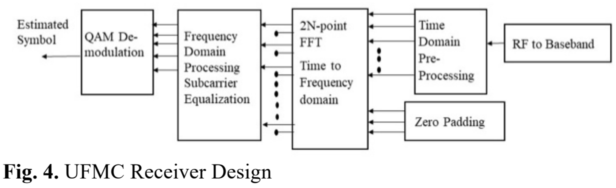

Fig. 4. UFMC Receiver Design

As a UFMC symbol has a length (N +L− 1), the missing samples N-L-1 are padded with zeros. Then, 2N-point FFT is considered to recover the data to transfer in the frequency region. Equalization and frequency domain processing are done. After QAM demodulation, the original data bits are retrieved.

3.3 Filtered OFDM

F-OFDM is the most adaptable waveform for 5G, with the customized numerology of different time-frequency grids to meet certain channel conditions and applications [27]. Using OFDM modulation, the bandwidth of F-OFDM is divided into discrete sub-bands in the time domain. Let us consider an F-OFDM system containing P subcarriers divided into B sub-bands in the time domain, with each sub-band transmitting M contiguous subcarriers, i.e., P = M·B. Figure 5 depicts the F-OFDM transmitter scheme.

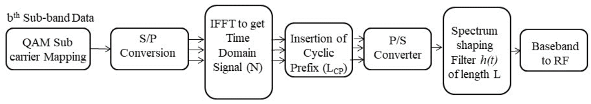

Fig. 5. F-OFDM Transmitter Block

Let the generated symbols be transmitted in each sub-band represented in vector form as equation (9):

$$S = [s_1, s_2, s_3, \dots, s_B]_{P\times 1} \tag{9}$$

The signal transmitted in the bth sub-band is represented as s_b as equation (10):

$$s_b = [s_b(1), s_b(2), \dots, s_b(M)]^T_{M\times 1} \tag{10}$$

The transmitter applies a CP and length-N IFFT of M QAM modulated data symbols throughout each OFDM symbol cycle. [28]. LCP presents the CP size. Therefore, the F-OFDM signal is created by combining OFDM sub-symbols at each of the lengths of M + LCP [29]. The resultant F-OFDM signal is passed through a suitably designed filter h(t) of the length L. The length of the filter should be set to half of the OFDM symbol length. Windowed sinc functions are used in the filtering operation [30]. In the system design, a low-pass Finite Impulse Response (FIR) filter is designed to truncate the sinc function by a Hanning window. The truncation of the Sinc filter is shown in equation (11):

$$h_B(t) \triangleq sinc_B(t)\cdot w(t) \tag{11}$$

The window has smooth transitions to zero on both ends to avoid the frequency leakage in the truncated filter [31]. Generalized expression for the applied window w(t) is given by equation (12):

$$w(t) = \begin{cases} 0.5\,[1+\cos(\frac{2\pi t}{L})]^{\alpha}, & |t| \le \frac{L}{2} \\ 0, & |t| > \frac{L}{2} \end{cases} \tag{12}$$

where α is the roll-off factor.

4. Polar Coding

Polar coding uses channel polarization to transform primary channels into virtual channels [32]. Channel polarization synthesizes W BMS channels out of X independent copies of a given channel. The new synthetic channels are then polarized in concerning the different transmission reliability. If the number of polarized channels is large enough, the channels are completely noisy or perfectly noiseless channels. Mutual information of the synthetic channels is either close to 0 or close to 1 [33]. For BMS channels, the index ‘i’ set I ∈ {1, 2, · · ·, E} is called the information set, and the value of these fixed positions are called frozen bits (F). Polar code is defined by its channel transformation matrix GN = G2⊗n, i.e., as the nth Kronecker power of the polarizing matrix G2, also called polarization kernel, n=log2E.

Polar Coding Algorithm [34]:
Input Parameters

Code Length	: E
polarizing matrix G_2	: $\begin{bmatrix} 1 & 0 \\ 1 & 1 \end{bmatrix}$
Transformation Matrix order	: n =$\log_2 E$
Input Information bits	: A
Code Rate	: R=(A/E)
Information vectors to encode	: c = [c_1, c_2…, c_A
Message Vector (Auxiliary)	: u = [u_1, u_2…., u_E
Index vector of information bit	: I ∈ {1, 2, · · ·,
Index vector of Frozen bit	: F

begin

$G_E = G_2^{\otimes n}$ %Channel transformation matrix; G_N is NxN matrix

d= [d_1, d_2…, d_E] = u · G_E %Codeword

W={$\boldsymbol{W}_E^{(1)}, \boldsymbol{W}_E^{(2)}, .., \boldsymbol{W}_E^{(E)}$ } *% Set of N synthetic channels*

Output:

x= d. W % Polarized output

There are a variety of algorithms for decoding polar-encoded messages. Arikan proposed the Successive Cancellation (SC) technique in [13] as one of the first decoding algorithms. Every time at the decoding stage in SC, it decides whether to proceed down the current path or turn around to locate a new, more reliable one. Each node at each level gives the hard decision vector β and receives soft information from its parent node α vector in logarithmic likelihood ratios (LLRs). The depth of the tree is first investigated, emphasizing the left branches [35]. SC decoding is suitable for more considerable block lengths. Successive Cancellation List (SCL) Decoding is employed to resolve this issue. Many possible pathways will be gathered and listed during the SCL decoding process. One path is chosen from the decoding paths in the SC decoder, but the L_P of the best decoding paths is activated and maintained simultaneously in the SCL decoder [36]. SCL becomes more efficient as the list grows, but its implementation becomes more difficult. Consideration of CRC-assisted (CA)-SCL can enhance the performance of the SCL decoding.

5. Massive MIMO Processing

In 5G massive MIMO systems, gNB is equipped with NR receiving antennas with digital transceiver chains capable of spatially multiplexing NT transmitting antennas. Massive MIMO system’s uplink is implemented where there are more receiving antennas than transmitting antennas: $N_R/N_T > 1$ [37]. The concept of beamforming in massive MIMO is applied. An antenna array of NR omni elements, with a spacing of λ/2 (½ wavelength) between the antenna elements, is used. The channel matrix H is deterministic, where h_{ij} is the channel gain from transmit antenna j to receive antenna i [38]. The matrix form is shown in equation (13):

$$H = \begin{bmatrix} h_{11} & h_{12} & \dots & h_{1N_T} \\ h_{21} & h_{22} & \cdots & h_{2N_T} \\ \vdots & \dots & \ddots & \vdots \\ h_{N_R1} & h_{N_R2} & \cdots & h_{N_RN_T} \end{bmatrix} \quad (13)$$

To identify the intended signal, all interference signals are reduced or eliminated by multiplying an appropriate weight matrix W, thereby inverting the channel's effect and representing each detected symbol as a linear combination of receiving signals [39]. In the system, zero forcing detects the signal where interferences are nullified by weight matrix W_{ZF} represented in equation (14), called the Moore-Penrose pseudo-inverse of H.

$$W_{ZF}=(H^H H)^{-1} H^H \quad (14)$$

6. System Model Novelty and Simulation

Unlike existing studies focusing on individual waveforms, this research offers a holistic approach by designing and analysing the performance of multiple waveforms—F-OFDM, FBMC, and UFMC within the 5G NR framework. This enables a comparative assessment and highlights their suitability for diverse 5G scenarios. The article presents the first-of-its-kind analysis that combines Polar coding with multiple waveforms, such as F-OFDM, FBMC, and UFMC, within a unified framework. While most research emphasizes macrocell applications, this work addresses small-cell deployment scenarios crucial for achieving the ultra-dense network configurations envisioned in 5G.

The system design is based on the model implemented in [40], where the Polar-coded Generalized Frequency Division Multiplexing (PC-GFDM) systems are designed. The system model is inspired from the proposed PC-FOFDM system presented in [41]. The 5G waveforms are implemented in Polar-coded representative Third Generation Partnership Project (3GPP) channel models to analyse the overall system performance under a 5G NR framework. The transmitter and receiver sections are shown in Figures 6 and 7. The simulation is done using MATLAB software version 2022b. It is divided into three stages. Firstly, the FBMC waveform analysis with standard numerology is presented. Further, the Polar-coded FBMC-OQAM system is simulated to observe the impact of QAM order on BER performance.

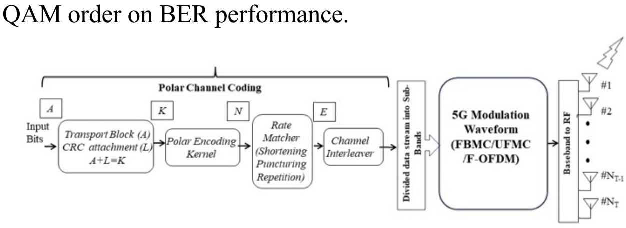

Fig. 6. Polar Coded Modulation Waveform Massive MIMO Uplink Design.

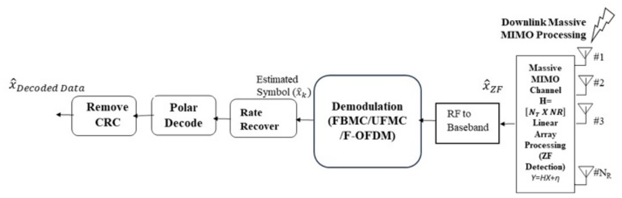

Fig. 7. Polar-Coded Massive MIMO Downlink

Firstly, the filters used in FBMC, UFMC, and F-OFDM modulation waveforms are simulated, and their time and frequency domain characteristics are shown in the following figure. The time domain filter characteristics for FBMC, F-OFDM, and UFMC are depicted in Fig. 8, Fig. 9, and Fig. 10. (a). The PHYDYAS filter is one of the best from the frequency spectrum of filters, with fewer out-of-band harmonics.

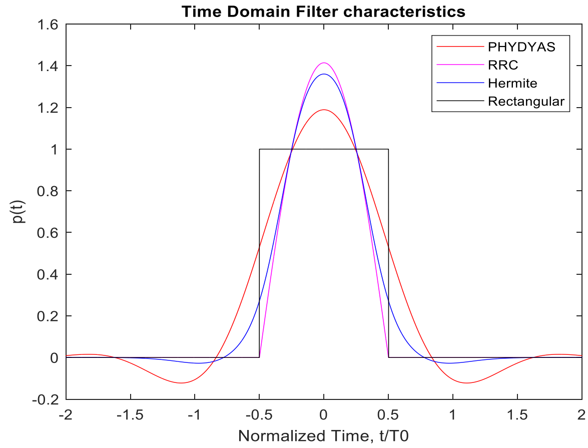

a)

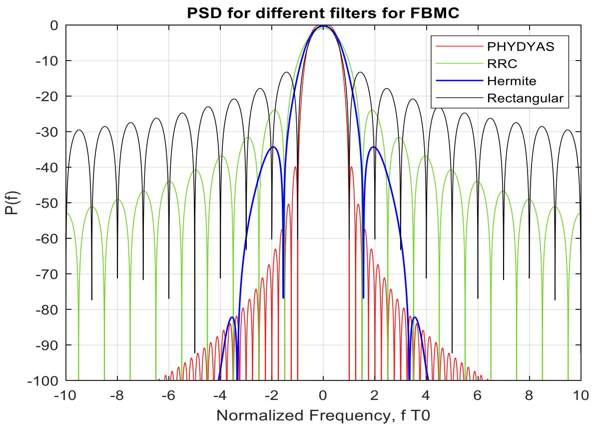

b)

Fig. 8. (a) FBMC Time Domain Filter Characteristics (b) PSD of Filter used in FBMC

Finally, the comprehensive system of the polar-coded waveform in a massive MIMO channel model is simulated. Table 2 presents the simulation parameters.

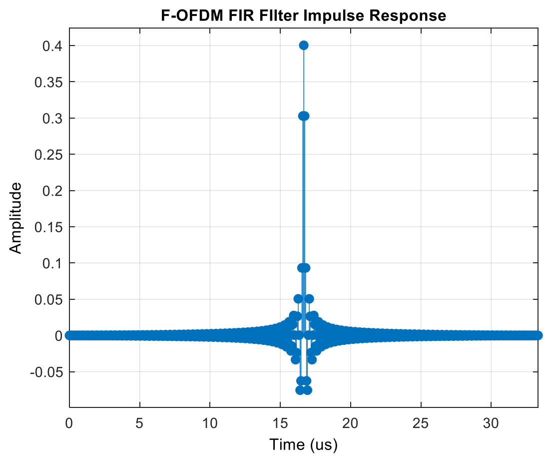

a)

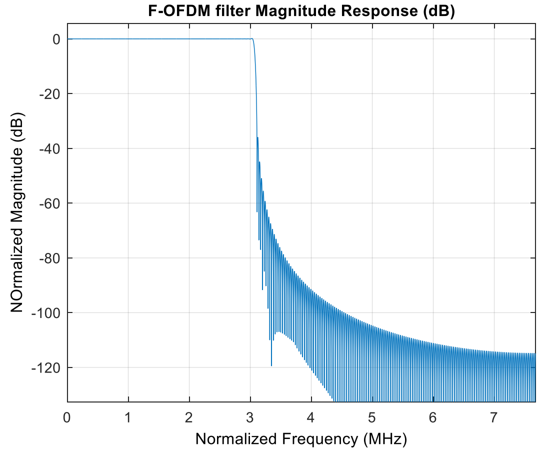

b)

Fig. 9. (a) F-OFDM time domain Filter characteristics (b) F-OFDM Frequency Filter Characteristics

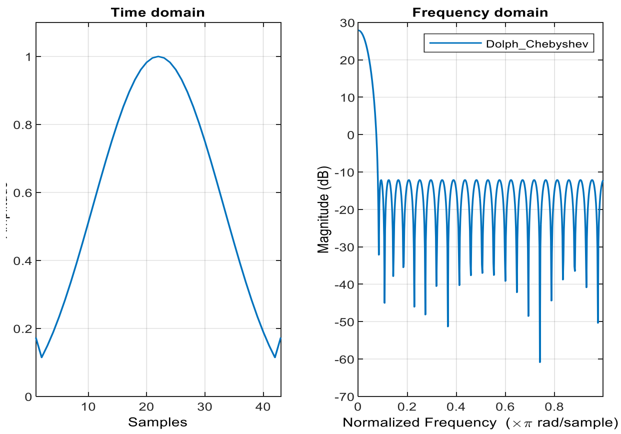

Fig 10. Filter characteristics used in UFMC with filter length L=43 and α=40

Table 2. List of Simulation Parameters

Parameter	Value
Common Waveform Parameters	
Number of Sub-bands	10
QAM order	64, 256
Size of FFT	512/1024
FBMC Parameters	
F-OFDM Parameters	
Number of Sub carriers	12
Overlapping factor K	4
Type of Filter	PHYDYAS
Filter length	43
Sub-carrier spacing	15KHz
Sideband filter attenuation	40 dB
F-OFDM Parameters	
Filter	Sinc the Hanning window
Number of sub-carriers/ Sub-band	20
Filter Length	513
CP length	32
Tone offset	2.5
UFMC Parameters	
Filter	Dolph-Chebyshev
Filter Length	43
Sub-band size	20
Sub-band Offset	156
Side lobe attenuation (α)	40dB

Massive MIMO channel Parameters	
Number of Antenna at Tx (NT)	16
Number of Antenna at Rx (NR)	20
Polar Coding Parameters	
Decoding List length (L)	8
Code rate R	1/2
Message length K	132
Rate matched output length	256

Figure 11 depicts the PSD for the 5G NR waveforms: FBMC, F-OFDM, and UFMC. In FBMC, the factor K impacts the PSD. The Spectral performance improves as the overlapping factor increases.

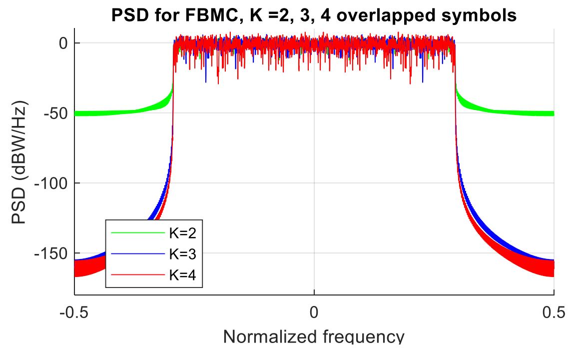

(a)

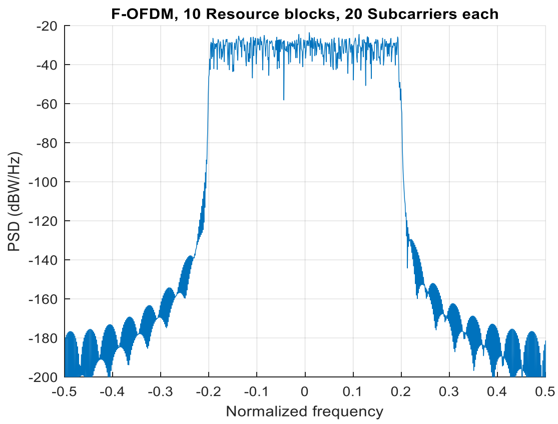

(b)

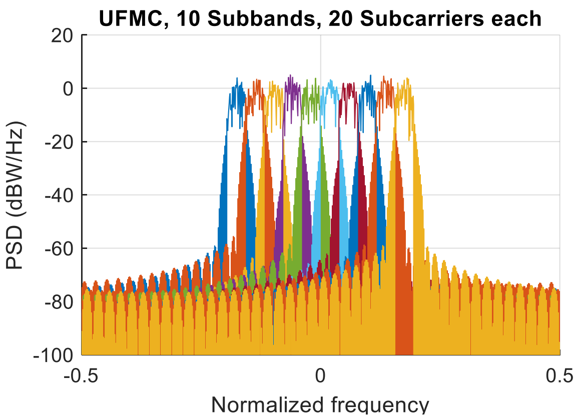

(c)

Fig. 11. PSD for (a) FBMC, (b) F-OFDM, (c) UFMC

Figure 12 compares FBMC, UFMC, and F-OFDM using the BER metric with different QAM orders. The BER curves prove that the BER performance degrades as the QAM order increases. Also, the highest BER is for the FBMC waveform, while F-OFDM outperforms FBMC and UFMC with an approximate SNR gain of ~4dB. To enhance this, Polar coding is implemented further.

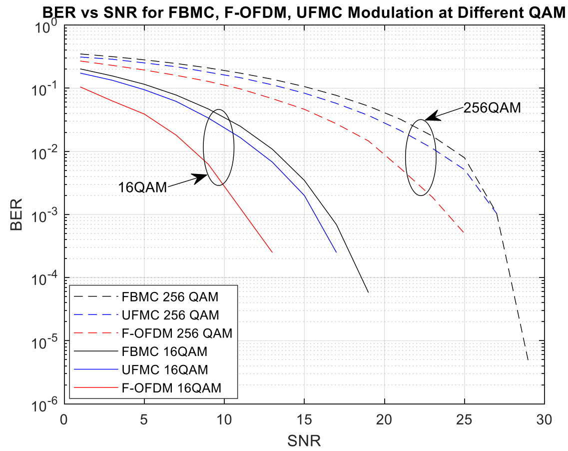

Fig. 12. BER Performance of FBCM, UFMC, F-OFDM with variable QAM order.

Figures 13 and 14 show the BER analysis of FBMC-OQAM with the BER performance in different MIMO setups. The significant finding is that as the MIMO antenna array size increases from 32 to 128, the SNR required to achieve the BER of 10^{-5} reduces from 30 dB to 22 dB. Further, the performance is enhanced by applying the polar coding in UFMC and F-OFDM, as depicted in Figures 15 and 16.

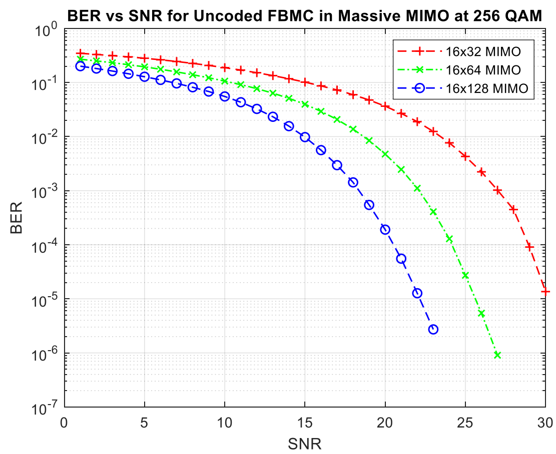

Fig. 13. BER performance Comparison for Uncoded and Polar Coded FBMC-OQAM with PHYDYAS Filter in variable MIMO setup

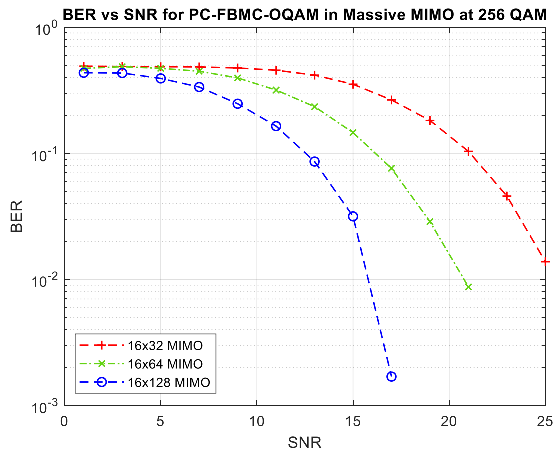

Fig. 14. BER performance Polar Coded FBMC-OQAM with PHYDYAS Filter

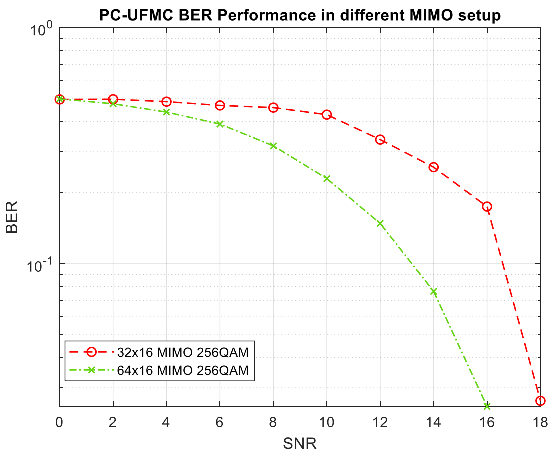

Fig. 15. BER performance for Polar Coded UFMC waveform in variable MIMO setup

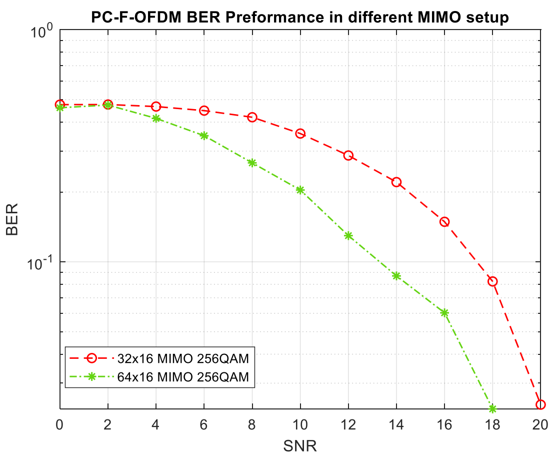

Fig. 16. BER performance for Polar Coded F-OFDM waveform in variable MIMO setup

The simulation of the Polar coded waveforms in the Massive MIMO scenario presented in Figures 14, 15, and 16 proved that UFMC is the best technique in terms of BER compared to FBMC and F-OFDM. The results for UFMC is far better than the results mentioned in [42-44]. The concluding remarks from the BER curve are presented in Table 3.

Table 3. BER Comparative Concluding Remarks

Modulation Waveform /MIMO Size	SNR Required to achieve BER=10^{-2} 32x16	64x16
FBMC	32 dB	19 dB
UFMC	18 dB	16 dB
F-OFDM	20 dB	18 dB

7. Conclusion

This paper simulates and analyzes the polar-coded 5G NR waveforms for BER. The analytical framework for the polar coded FBMC, UFMC, and F-OFDM in massive MIMO scenarios is designed. Under this framework, the BER performance at higher-order QAM is proposed. Integrating Polar coding with advanced waveform techniques (F-OFDM, FBMC, UFMC) in small-cell networks offers a comprehensive foundation for addressing the challenges of 5G networks. The system is designed in different MIMO antenna setups to enhance the BER performance. Simulation results proved that the proposed polar-coded UFMC system performs better than FBMC and F-OFDM. Polar-coded UFMC achieves SNR gain of approximately ~2dB and ~12 dB, respectively, over F-OFDM and FBMC waveforms in 32x16 MIMO setup. The FBMC is the most spectrally efficient technique, and when integrated with NR-based polar coding in massive MIMO scenarios, the BER performance is degraded compared to other methods.

Various factors like spectral efficiency, PAPR, system capacity, etc., can be explored for the proposed hybrid polar-coded Massive MIMO systems. In the future, the design can be extended further to operate in the terahertz efficient (THz) frequency range, which is crucial for 6G communication. Polar codes can be combined with other advanced coding techniques (e.g., LDPC or Turbo codes) to improve error correction for specific scenarios. To develop intelligent beamforming algorithms that use AI and deep learning can be explored to enhance spatial resolution and reduce interference.

References

[1] F. Qamar, M. U. A. Siddiqui, M. N. Hindia, R. Hassan, and Q. N. Nguyen, "Issues, Challenges, and Research Trends in Spectrum Management: A Comprehensive Overview and New Vision for Designing 6G Networks," *Electronics*, vol. 9, no. 9, Sep. 2020, Art. no. 1416, doi: 10.3390/electronics9091416.

[2] M. Shirvanimoghaddam *et al.*, "Short Block-Length Codes for Ultra-Reliable Low Latency Communications," *IEEE Commun. Mag.*, vol. 57, no. 2, pp. 130–137, Feb. 2019, doi: 10.1109/mcom.2018.1800181.

[3] *5G; Service requirements for the 5G system*, Technical Specification 3GPP TS 22.261, 650 Route Des Lucioles F-06921 Sophia Antipolis Cedex - France., 2021. [Online]. Available: https://www.etsi.org/deliver/etsi_ts/122200_122299/122261/15.09.00_60/ts_122261v150900p.pdf

[4] M. Eiman, "Minimum Technical Performance Requirements for IMT-2020 radio interface(s)," presented at the ITU-R Workshop on IMT-2020, Brussels, Belgium, 2020. [Online]. Available: https://www.itu.int/en/ITU-R/study-groups/rsg5/rwp5d/imt-2020/Documents/S01-1_Requirements%20for%20IMT-2020_Rev.pdf

[5] M. Elkourdi, B. Pekoz, E. Guvenkaya, and H. Arslan, "Waveform design principles for 5G and beyond," in *2016 IEEE 17th Annual Wirel. Microw. Techn. Conf. (WAMICON)*, Clearwater, FL: IEEE, Apr. 2016, pp. 1–6. doi: 10.1109/wamicon.2016.7483859.

[6] X. Zhang, L. Chen, J. Qiu, and J. Abdoli, "On the Waveform for 5G," *IEEE Commun. Mag.*, vol. 54, no. 11, pp. 74–80, Nov. 2016, doi: 10.1109/mcom.2016.1600337cm.

[7] F. Schaich, T. Wild, and Y. Chen, "Waveform Contenders for 5G - Suitability for Short Packet and Low Latency Transmissions," in *2014 IEEE 79th Vehicular Techn. Conf. (VTC Spring)*, Seoul, South Korea: IEEE, May 2014. doi: 10.1109/vtcspring.2014.7023145.

[8] "5Gnow.eu » alles über Tarife, Handys & Flatrates im 5G-Netz," 5Gnow. Accessed: May 01, 2025. [Online]. Available: https://www.5gnow.eu/

[9] A. Farhan, N. Marchetti, F. Figueiredo, and J. P. Miranada, "Massive MIMO and Waveform Design for 5th Generation Wireless Communication Systems," in *Proceed. 1st Int. Conf. 5G Ubiq. Connect.*, Levi, Finland: ICST, 2014. doi: 10.4108/icst.5gu.2014.258195.

[10] A. Sahin, I. Guvenc, and H. Arslan, "A Survey on Multicarrier

Communications: Prototype Filters, Lattice Structures, and Implementation Aspects," *IEEE Commun. Surv. Tutorials*, vol. 16, no. 3, pp. 1312–1338, 2014, doi: 10.1109/surv.2013.121213.00263.

[11] B. Khan and F. J. Velez, "Multicarrier Waveform Candidates for Beyond 5G," in *2020 12th Int. Symp. Commun. Sys., Netw. Dig. Sign. Proc. (CSNDSP)*, Porto, Portugal: IEEE, Jul. 2020, pp. 1–6. doi: 10.1109/csndsp49049.2020.9249568.

[12] A. J. Ramadhan, "Overview and Comparison of Candidate 5G Waveforms: FBMC, UFMC and F-OFDM," *Int. J. Comp. Netw. Inform. Sec.*, vol. 14, no. 2, pp. 27–38, Apr. 2022, doi: 10.5815/ijcnis.2022.02.03.

[13] A. S. Ahmed, H. Al-amaireh, and Z. Kollar, "Multicarrier Modulation Schemes for 5G Wireless Access," *ECTI-CIT Trans.*, vol. 16, no. 4, pp. 378–392, Sep. 2022, doi: 10.37936/ecti-cit.2022164.248710.

[14] R. Anil Kumar, Kodati Satya Prasad, "Comparative Analysis of OFDM, FBMC, UFMC & GFDM for 5G Wireless Communications", *Int. J. Adv. Sci. Techn.*, vol. 29, no. 05, pp. 2097 - 2108, Apr. 2020.

[15] R. Chataut and R. Akl, "Massive MIMO Systems for 5G and beyond Networks—Overview, Recent Trends, Challenges, and Future Research Direction," *Sensors*, vol. 20, no. 10, May 2020, Art. no. 2753, doi: 10.3390/s20102753.

[16] S. Nilofer and P. K. Malik, "5G Multi-Carrier Modulation Techniques: Prototype Filters, Power Spectral Density, and Bit Error Rate Performance," Mar. 24, 2021, *Research Square Platform LLC*. doi: 10.21203/rs.3.rs-345216/v1.

[17] T. L. Marzetta, "Noncooperative Cellular Wireless with Unlimited Numbers of Base Station Antennas," *IEEE Trans. Wireless Commun.*, vol. 9, no. 11, pp. 3590–3600, Nov. 2010, doi: 10.1109/twc.2010.092810.091092.

[18] "The Road to 5G: Drivers, Applications, Requirements and Technical Development," GSA. Accessed: May 01, 2025. [Online]. Available: https://gsacom.com/paper/the-road-to-5g-drivers-applications-requirements-and-technical-development/

[19] A. Sharma and M. Salim, "Polar Code Appropriateness for Ultra-Reliable and Low-Latency Use Cases of 5G Systems," *Int. J. Network. Distrib. Comp.*, vol. 7, no. 3, 2019, Art. no. 93, doi: 10.2991/ijndc.k.190702.005.

[20] D. Hui, S. Sandberg, Y. Blankenship, M. Andersson, and L. Grosjean, "Channel Coding in 5G New Radio: A Tutorial Overview and Performance Comparison with 4G LTE," *IEEE Veh. Technol. Mag.*, vol. 13, no. 4, pp. 60–69, Dec. 2018, doi: 10.1109/mvt.2018.2867640.

[21] M. Van Eeckhaute, A. Bourdoux, P. De Doncker, and F. Horlin, "Performance of emerging multi-carrier waveforms for 5G asynchronous communications," *J Wireless Com Network*, vol. 2017, no. 1, pp. 1 – 15, Dec. 2017, doi: 10.1186/s13638-017-0812-8.

[22] A. Ijaz, L. Zhang, P. Xiao, and R. Tafazolli, "Analysis of Candidate Waveforms for 5G Cellular Systems," in *Towards 5G Wireless Networks*, H. K. Bizaki, Ed., Rijeka: IntechOpen, 2016. doi: 10.5772/66051.

[23] T. Ihalainen, T. Hidalgo Stitz, M. Rinne, and M. Renfors, "Channel Equalization in Filter Bank Based Multicarrier Modulation for Wireless Communications," *EURASIP J. Adv. Signal Process.*, vol. 2007, no. 1, Dec. 2006, doi: 10.1155/2007/49389.

[24] V. Vakilian, T. Wild, F. Schaich, S. Ten Brink, and J.-F. Frigon, "Universal-filtered multi-carrier technique for wireless systems beyond LTE," in *2013 IEEE Globecom Workshops (GC Wkshps)*, Atlanta, GA: IEEE, Dec. 2013. doi: 10.1109/glocomw.2013.6824990.

[25] L. Sakkas, E. Stergiou, G. Tsoumanis, and C. T. Angelis, "5G UFMC Scheme Performance with Different Numerologies," *Electronics*, vol. 10, no. 16, Aug. 2021, Art. no. 1915, doi: 10.3390/electronics10161915.

[26] S. Jolania, R. Sindal, and A. Saxena, "Performance of UFMC Waveform Design implemented in Massive MIMO system for 5th Generation Wireless Communication Systems," in *2022 4th Int. Conf. Adv. Comp., Commun. Contr. Network. (ICAC3N)*, Greater Noida, India: IEEE, Dec. 2022, pp. 1732–1736. doi: 10.1109/icac3n56670.2022.10074534.

[27] J. Abdoli, M. Jia, and J. Ma, "Filtered OFDM: A new waveform for future wireless systems," in *2015 IEEE 16th Int. Worksh. Sign. Proces. Adv. Wirel. Commun. (SPAWC)*, Stockholm, Sweden: IEEE, Jun. 2015. doi: 10.1109/spawc.2015.7227001.

[28] A. J. R. Al-Aameri, "Secure Slicing and Allocation of Resources of 5G Networks In Software-Defined Networking / Network Functions Virtualization," *IIUM Eng. J.*, vol. 23, no. 2, pp. 85–103, Jul. 2022, doi: 10.31436/iiumej.v23i2.1763.

[29] L. Zhang, A. Ijaz, P. Xiao, M. M. Molu, and R. Tafazolli, "Filtered OFDM Systems, Algorithms, and Performance Analysis for 5G and Beyond," *IEEE Trans. Commun.*, vol. 66, no. 3, pp. 1205–1218, Mar. 2018, doi: 10.1109/tcomm.2017.2771242.

[30] Z. Dong, "F-OFDM scheme and filter design," *Cutting Edge*, no. 80, pp. 63–68, May 2016.

[31] "3GPP TDocs (written contributions) at meeting." Accessed: February 01, 2025. [Online]. Available: https://www.3gpp.org/dynareport?code=TDocExMtg--R1-85--31662.htm

[32] W. Yongxue, W. Sunan, and W. Weiqiang, "Performance Analysis of the Universal Filtered Multi-Carrier (UFMC) Waveform for 5G System," *J. Phys.: Conf. Ser.*, vol. 1169, Feb. 2019, Art. no. 012065, doi: 10.1088/1742-6596/1169/1/012065.

[33] V. Bioglio, C. Condo, and I. Land, "Design of Polar Codes in 5G New Radio," *IEEE Commun. Surv. Tutorials*, vol. 23, no. 1, pp. 29–40, Jan. 2021, doi: 10.1109/comst.2020.2967127.

[34] Z. Babar *et al.*, "Polar Codes and Their Quantum-Domain Counterparts," *IEEE Commun. Surv. Tutorials*, vol. 22, no. 1, pp. 123–155, Jan. 2020, doi: 10.1109/comst.2019.2937923.

[35] E. Arikan, "Channel Polarization: A Method for Constructing Capacity-Achieving Codes for Symmetric Binary-Input Memoryless Channels," *IEEE Trans. Inform. Theory*, vol. 55, no. 7, pp. 3051–3073, Jul. 2009, doi: 10.1109/tit.2009.2021379.

[36] A. Balatsoukas-Stimming, A. J. Raymond, W. J. Gross, and A. Burg, "Hardware Architecture for List Successive Cancellation Decoding of Polar Codes," *IEEE Trans. Circuits Syst. II*, vol. 61, no. 8, pp. 609–613, Aug. 2014, doi: 10.1109/tcsii.2014.2327336.

[37] K. Niu and K. Chen, "CRC-Aided Decoding of Polar Codes," *IEEE Commun. Lett.*, vol. 16, no. 10, pp. 1668–1671, Oct. 2012, doi: 10.1109/lcomm.2012.090312.121501.

[38] H. Hu, H. Gao, Z. Li, and Y. Zhu, "A Sub 6GHz Massive MIMO System for 5G New Radio," in *2017 IEEE 85th Vehicular Techn. Conf. (VTC Spring)*, Sydney, NSW: IEEE, Jun. 2017, pp. 1–5. doi: 10.1109/vtcspring.2017.8108327.

[39] K. Zheng, S. Ou, and X. Yin, "Massive MIMO Channel Models: A Survey," *Int. J. Ant. Propag.*, vol. 2014, pp. 1–10, Apr. 2014, doi: 10.1155/2014/848071.

[40] Y. Li, K. Niu, and C. Dong, "Polar-Coded GFDM Systems," *IEEE Access*, vol. 7, pp. 149299–149307, Jul. 2019, doi: 10.1109/access.2019.2947254.

[41] T. Deepa and N. Bharathiraja, "Performance Evaluation of Polar Coded Filtered OFDM for Low Latency Wireless Communications," *Wireless Pers. Commun.*, vol. 116, no. 3, pp. 2023–2034, Feb. 2021, doi: 10.1007/s11277-020-07777-2.

[42] G. K. Sharma, R. K. Arya, and V. S. Nigam, "Performance Analysis of UFMC for 5G Technologies with Different Channel Coding Techniques," in *2023 Int. Conf. Sign. Process., Comput., Electr., Power Telecommun. (IConSCEPT)*, Karaikal, India: IEEE, May 2023, pp. 1–6. doi: 10.1109/iconscept57958.2023.10170587.

[43] T. A. Abose, F. O. Ayana, T. O. Olwal, and Y. W. Marye, "BER performance analysis of polar-coded FBMC/OQAM in the presence of AWGN and Nakagami-m fading channel," *AIMS Electr. Electrical Eng.*, vol. 8, no. 3, pp. 311–331, Mar. 2024, doi: 10.3934/electreng.2024014.

[44] "Design of Polar Coding in Filtered-OFDM," in *Lecture Notes in Electrical Engineering*, Singapore: Springer Nature Singapore, 2023, pp. 583–593. doi: 10.1007/978-981-99-0416-7_58.